JAXA-ONERA-DLR Cooperation: Results from Acoustic Optimizations of a Rotor in Descent Flight

Gunther Wilke
German Aerospace Center (DLR), Braunschweig, Germany
Joëlle Bailly
The French Aerospace Lab (ONERA), Meudon, France
Yves Delrieux
The French Aerospace Lab (ONERA), Châtillon, France
Keita Kimura, and Yasudata Tanabe
Japan Aerospace Exploration Agency (JAXA), Tokyo, Japan

1 Introduction

In 2019, JAXA, ONERA and DLR have joined forces to cooperate on the optimization of helicopter rotor blades. The cooperation aims to further understand rotor aerodynamics and enhance and validate the tools for simulation and optimization of the planform and twist of rotor blades in various flight conditions. After optimizing the required power in hover (Ref. 1) and high advance ratio flight (Ref. 2) separately, a combined optimization of both was presented in 2023 (Ref. 3). This work presents the challenges with modelling the descent flight condition to capture the noise generated by blade-vortex interaction and means to reduce this phenomenon. The aim is to identify suitable means and methods for the acoustic optimization of helicopter rotors in descent flight.

2 Literature Review

The field of rotor acoustics is large and many insights have been gained over the years. For example Splettstößer et al. (Ref. 4) put together a database for understanding the noise generation of a classical helicopter. Two key flight conditions are identified, namely fast forward flight with the advent of high-speed impulsive noise caused by shocks forming on the advancing side; and descent flight where mostly parallel blade-vortex interaction causes noise due to the fluctuation of inflow and therefore forces on the rotor. DLR and ONERA then went on to jointly developed the ERATO blade (Ref. 5), (Ref. 6). The idea behind the ERATO blade is to reduce BVI noise passively through an altered planform. The blade features a double-sweep, which reduced the parallelism to the vortices encountered, but also has an impact on the vortex miss distance. Latter is a key driver for BVI acoustics. This leads to also a shift of the noise towards level flight, however the overall trade-off seems to be justified. In the reference condition, a reduction of up to 4 dB A with respect to the reference blade, 7AD (Ref. 7), has been observed. The ERATO blade has then been further developed into the Blue Edge™ blade (Ref. 8), now being operated on the H160 helicopter by Airbus Helicopters. Airbus Helicopters also transferred this technology to the H225 helicopter (Ref. 9). Generally, passive blade design has the advantage that it is maintenance free. A good overview of the various trends can be found in Brocklehurst and Barakos (Ref. 10), which is not limited to pure aero-acoustic consideration.

Opposing passive designs, various studies exist that investigate the effect of active systems. A renowned wind tunnel campaign is HART II (Ref. 11), which utilized a higher harmonic control system to either minimize noise or vibrations based on a scaled Bo105 blade. The minimum noise operation case reduces the BVI related sound pressure level (SPL) by about 1 dB. JAXA and KARI (Ref. 12) test a model blade with an active tab mechanism and show a potential reduction of 3.3 dB in BVI SPL when choosing the optimal phase and actuation amplitude. In the ongoing STAR II project (Ref. 13), a similar noise reduction is predicted as for the HART II blade using active twist, but this will need to be confirmed by the wind tunnel test. Looking at the multi-swash plate experiment by DLR (Ref. 14), the benefit of an active system is proven. For a scaled Bo105 blade, a reduction of 4.5 dB could be achieved, while a more modern blade design based on a scaled EC145 reduces this number slightly to 3.9 dB.

Besides the actual technologies to mitigate the helicopter noise, the simulation methodologies to design this blade are also quickly reviewed, be it passive or active. A common tool to predict the acoustics for rotor blade is the application of the Ffowcs-Williams Hakwins equations (FW-H) in any of the Farassat formulations (Ref. 15). This method requires the input of a pressure surface that can potentially even be simplified to a line. This data may then be obtained either by experiment or numerical simulation. The rotorcraft community may be split into two categories to compute these blade pressure/loads. The first category utilizes comprehensive codes with prescribed or free-wake models, whereas the second category utilizes computational fluid dynamics (CFD) coupled with comprehensive codes. The advantage of the wake methods is their speed; however, they require careful fine tuning of the vortex core radius modelling, but also their representation of the tip vortices often achieved by roll-up models. Opposing this, CFD methods require some form of numerical dissipation to become stable, but also coarse computational grids may induce more numerical dissipation as wanted. The numerical dissipation leads to a too early diffusion of the tip vortices and therefore needs to be carefully mitigated through the application of many grid points, higher order schemes and advanced turbulence modeling.

Jones and Burley (Ref. 16) set up a numerical tool chain to compute helicopter noise, where the blade loading obtained from a comprehensive code is utilized as input to a FW-H tool, but may opposingly be produced by CFD in the form of a pressure surface. When using a comprehensive codes in conjunction with a wake model, the core vortex modelling has to be carefully adjusted and tip-roll up models have been developed to capture the distinct BVI phenomenon. Examples can be found by Brookes et al. (Ref. 17) or Rahier and Delrieux (Ref. 18). The work by Rahier and Delrieux has then be incorporated into an acoustic prediction toolchain by Beaumier and Delrieux (Ref. 19). They freeze the original comprehensive code trim and motion of the blade obtained with a simple free-wake code, to then re-develop the wake with the improved wake modelling. This in turn is then used to determine the inflow for 2D inviscid and incompressible calculations of the airfoil sections, which are Prandtl-Glauert corrected to account for compressibility. From these 2D calculations, a pressure surface is generated to be used by their FW-H tool. With this toolchain, they arrive at a reasonable agreement with the experiment, but are orders of magnitude faster than CFD based predictions. Duque et al. (Ref. 20) demonstrate that CFD based BVI predictions improved the accuracy by employing techniques such as a higher than 2^{nd} order inviscid flux computation, adaptive mesh refinement, and advanced turbulence modeling (DES). Lim and Dimanlig (Ref. 21) demonstrate such methods for the HART II case and highlight the inclusion of the fuselage to obtain a correct blade trim, which is necessary to capture the correct vortex miss distance. van der Wall et al. (Ref. 22) and Smith et al. (Ref. 23) compare methods from the HART II consortium in their ability to correctly capture the BVI noise (besides general aero-mechanical modeling of the blades). A way to combine the efficient wake preservation of free wake methods with CFD are hybrid methods as for example presented by JAXA (Ref. 24). Jain et al. (Ref. 25) demonstrate through accurate CFD simulations, the correlation of unsteady airloads as required for FW-H codes is highly improved through the application of higher order schemes, high grid resolution and small time steps. Kowarsch et al. (Ref. 26) obtain a good match with a flight experiment of a H145 helicopter within an accuracy of 3.5 dB ENPL (effective noise level perceived) in a certification flight condition. They employ a 6th order WENO scheme in combination with many grid points to arrive at this accuracy. Wilke (Ref. 27) shows that the noise prediction becomes more accurate by employing a 4^{th} order Pade scheme in background mesh for the HART II blade over simply using 2^{nd} order central schemes, but additionally being able to employ higher order methods in the whole field delivers further improvements (Ref. 28). A similar comparison is done by DLR and JAXA (Ref. 29), which demonstrate that the application of refined grids and higher order schemes is beneficial to correctly predict the acoustics of a rotor. A recent study by Hong et al. (Ref. 30) compares a MUSCL reconstruction and a WENO reconstruction for the HART II blade, where a newly refined sensor system allows the MUSCL reconstruction to surpass WENO schemes of the same formal order.

While the correct simulation of the rotor acoustics is essential to arrive at a successful rotor design, the methods on how to arrive at a good design are also studied by various research groups. Baeder (Ref. 31) is among the first to optimize rotor blades using CFD, however his focus is on the high-speed impulsive noise in forward flight and different concepts are tried. Visingardi et al. (Ref. 32) apply a comprehensive code with an FW-H solver in a multi-point optimization to reduce the noise. They directly apply a multi-objective, evolutionary algorithm to find new blade designs that exploit a dual-speed system. Rabe (Ref. 33), Rabe and Wilke (Ref. 34) and Wilke (Ref. 28) compare different simulation strategies and their effectiveness in designing new blade planforms. While the final conclusion of these studies is that CFD is the most accurate methodology, a thoughtfully used low-fidelity method may be able to capture the trends sufficiently well. Another insight is that it is imperative to correctly model the blade motion given from elasticity and flight mechanics, as otherwise the resulting rotor blade may lead to be the exact opposite of what would be desirable. Their method to optimize the blades is based on surrogate-based optimization. The surrogate models are built from simulation data to then predict the metric to optimize at a fraction of computational cost to accelerate the optimization. Opposing the surrogate-based optimization route, the application of gradient optimizers becomes viable when the CFD based gradients can be evaluated using the adjoint method. For rotor acoustics, Fabiano and Mavripilis (Ref. 35), and Wang et al. (Ref. 36) are the first to demonstrate such capabilities for unsteady simulations. However, their applied grid densities and the applied numerical order are too little to sufficiently capture BVI. The reason is the enormous amount of data that needs to be stored for applying the adjoint to unsteady problems. Fitzgibbon (Ref. 37), and Fitzgibbon et al. (Ref. 38) demonstrate their harmonic balance approach to overcome this somewhat. However, for BVI related problems, up to 40 times the rotor frequency need to be captured and are therefore likely too memory consuming to solve. In contrast, on the mid-fidelity side, Chia et al. (Ref. 39) optimize the Bo105 blade passively and actively using the surrogate based optimization technique. Recent industrial projects by Airbus Helicopters (Ref. 40), (Ref. 41) also utilize a mix of low-fidelity and CFD methods to analyze their designs.

In this paper, the surrogate-based optimization is investigated and various low/mid fidelity methods and CFD based approaches are investigated. The impact of elasticity is also studied with respect to the final blade shape.

3 Methodology

In order to speed up the optimization, surrogate models are employed. All partners used Kriging as their baseline surrogate (Ref. 61) in combination with global optimization algorithms, thus a derivative of the EGO algorithm (Ref. 62) for the optimization.

On the ONERA side (Ref. 19), a tool chain centered around a comprehensive code coupled with a free-wake code is applied to predict efficiently the acoustic noise of a helicopter rotor in blade-vortex interaction conditions. The method was improved by detecting tip vortices and then computing 2D sectional pressure distributions with a singularity method using the inflow from their enhanced free-wake model to generate an acoustic surface to be post-processed by an in-house FW-H code. Tanabe et al. (Ref. 63) developed CFD-CSD based rotor simulations for JAXA that can also be coupled with their FW-H code. DLR utilizes a mid-fidelity tool based on a panel method coupled with a free-wake code (UPM) (Ref. 42) or a high-fidelity CFD method (Ref. 47) to compute the acoustic pressure surface for the acoustic FW-H prediction. The partners applied the rigid as well as elastic blade assumptions to study the impact on the rotor acoustics, besides the impact of the various fidelities. Thus, it is also partially an extension of the works by Rabe and Wilke (Ref. 33), and Wilke (Ref. 64) by looking into various approaches on how to efficiently optimize a blade for descent flight acoustics.

In Table 1, the DLR and ONERA low-fidelity tool chains are briefly compared with each other. Both utilize Airbus Helicopters' HOST (Ref. 44) comprehensive code to compute the trim state, and both do only a one-way coupling with their respective aero-dynamic mid-fidelity tool. This means, the obtained blade motion is passed onto the next tool to compute blade pressures, but these are not used to correct the trim again. On the DLR side, the unsteady panel method (UPM (Ref. 42)) coupled with a free-wake code is employed. The fuselage is included for the UPM simulation, therefore the displacement effect of the fuselage is included during the computation of the blade pressures. However, it is absent in the HOST simulation as well as in the FW-H computation with APSIM (Ref. 45). ONERA carried out investigations by including elastic deformation and neglecting it, whereas DLR only presents its elastic optimization results. They utilize MENTHE (Ref. 18) to compute and improved wake and determine the onflow conditions for the 2D airfoil simulations with ARHIS (Ref. 43), to the hand the blade-pressures over to their FW-H code PARIS (Ref. 46).

Opposing this, the details of the CFD based high-fidelity approaches are listed in Table 2. DLR and JAXA studied the variation of results in dependency of the computational grid regarding the baseline blade, therefore the mesh settings for the optimization are underlined. Both of them apply the same upwinding scheme and very similar reconstructions, but different turbulence models. While DLR couples their CFD code FLOWer with HOST comprehensive code to account for elasticity, JAXA utilizes their rFlow3D CFD solver with its own trim procedure assuming rigid blades. ONERA also performed high-fidelity simulations based on CFD-CSD loose coupling between elsA and HOST to check a posteriori the acoustic performance of the different rotor blades at the nominal descent angle. ONERA relies on the conventional 2^{nd} order central JST scheme. A vorticity confinement method developed at ONERA (Ref. 65) has been applied to ensure vorticity preservation. DLR additionally models the fuselage following the improved results of the HART II rotor by Lim and Dimanlig (Ref. 21) when they included the fuselage in their simulations. DLR utilized the in-house meshing tool G^3 based on transfinite interpolation (Ref. 66), whereas the JAXA and ONERA grids were made using the commercial software Pointwise and ICEM, respectively. For the optimization, they utilized mesh deformation to reflect the geometrical changes, whereas DLR simply remeshed the new geometry.

4 Methods Comparison for Baseline Blade

Reference Rotor

The baseline rotor for the optimization studies is the HART II (Ref. 11) rotor in the corresponding baseline flight condition, where the higher harmonic controls have been disabled. The flight condition including reference numbers regarding this scaled Bo105 blade are listed in Table 3.

In this section, the low fidelity results will be presented first followed by CFD based high fidelity analysis to then contrast selected results in the end. While in the experiment the loudest measured case was at an descent angle $\gamma = -6.0°$, the chosen reference angle was $\gamma = -7.0°$ as it was found to be the loudest for the partners when using high-fidelity CFD. Unfortunately, this angle has not been measured in the experiment. In all cases, a wind

Table 1: Overview of low fidelity simulation methods. (FW-H (Ref. 15))

	DLR LoFi	ONERA LoFi
aerodynamics	UPM (Ref. 42)	MENTHE (Ref. 18) ARHIS (Ref. 43)
elastics & trim		HOST (Ref. 44)
acoustics (FW-H)	APSIM (Ref. 45)	PARIS (Ref. 46)
azimuth step $\Delta\psi$	1	1
chordwise points n_c	81	1
spanwise points n_r	17	20
elasticity	yes & no	yes & no
lam.-turb. transition	airfoil tables	airfoil tables
fuselage	yes	no

Table 2: Overview of high fidelity CFD based simulation. Underlined parameters highlight the values utilized during optimization.

CFD	DLR	JAXA	ONERA
aerodynamics	FLOWer (Ref. 47)	rFlow3D (Ref. 48)	elsA (Ref. 49)
elastics & trim	HOST (Ref. 44)	rMode (Ref. 48)	HOST (Ref. 44)
acoustics	APSIM (Ref. 45)		PARIS (Ref. 46)
azimuth step $\Delta\psi$	1.0,0.5,0.25	0.1	0.3
chordwise points n_c	81, 129, 257	129, 171, 251	80
spanwise points n_r	81, 129, 257	121, 161, 241	80
background grid			
spacing $\Delta x/c$	20%, 14%, 7%	20% 15%, 10%	20%
# points $\cdot 10^6$	5, 14, 102	14 28, 74	7
inviscid scheme	FCMT (Ref. 50) (Ref. 51)	and SLAU2m (Ref. 52) (Ref. 48)	JST (Ref. 53) and VC (Ref. 54)
turb. model	SA-DDES-R	SA-R (Ref. 55) (Ref. 56)	Kok $k-\omega$
	(Ref. 55) (Ref. 57) (Ref. 56)	(Ref. 58)	(Ref. 59)
elasticity	yes	no	yes
lam.-turb. transition	yes	no	no
transition	emperical (Ref. 60)	no	no

Table 3: Rotor parameters and baseline flight condition.

	HART-II
R	2 m
chord	0.121 m
twist	$-8^o/R$
airfoil	NACA 23012 with tab
M_{tip}	0.64
M_∞	0.097
descent angle γ	$-6^o = -4.5^o - 1.5^o$

tunnel correction of $\Delta\alpha_s = 1.5°$ has been applied, which may also be a source of inaccuracy.

Low Fidelity Results

At first, the low fidelity simulation methods by ONERA and DLR are compared against the baseline test case of the HART II rotor and therefore pose as an abbreviated assessment as done by van der Wall et al. (Ref. 67) for the respective methods utilized here. The low fidelity aerodynamic models are utilized and additionally an assessment of the impact of neglecting or including the elastics is given there. Therefore, the simulations are marked as either LoFiR or LoFiE for rigid or elastic simulations respectively. The retrieved trim control angles and according blade vortex interaction sound pressure levels (BVI SPL) are plotted in Fig. 1 over a sweep of descent angles, but also the sectional load derivative being the driver for acoustics. The most distinct observation about the trim control angles is that the rigid simulations tend to underpredict the collective pitch, which can roughly be explained by the lack of the mean torsional deformation of around 1° at the blade tip in contrast to the elastic simulations. For the BVI SPL curve, the ONERA results overshoot the peak noise slightly with respect to the experiment, while the DLR results are below the peak noise. The ONERA-LoFiR results however show a smooth rise and fall of the curve, while the ONERA-LoFiE result has a dent in the curve at $\gamma = -8°$ and $\gamma = -7°$. Opposing this, the DLR results are too quiet. The reason is that the tip core radius has been calibrated to remove dents as found in the ONERA-LoFiE results, while still maintaining the BVI hot spots on the noise carpets. Moving onto the sectional load derivative, in all cases it is observed that the advancing BVI is captured more strongly as seen in the strong oscillations between $\psi = 0..90°$, but also the retreating side is captured at for $\psi = 270..360°$. The ONERA results show a greater amplitude than the DLR and experimental results, which also explains the greater noise levels.

These azimuthal locations are roughly found again on the respective noise carpets, which are plotted along with the experimental noise carpet in Fig. 2. While the absolute value of the peak noise cannot be captured at high precision by the low fidelity methods, the two BVI hot spots as found in the experiment are found again for all simulations. The directivities are globally well replicated.

High Fidelity Grid Studies

JAXA carried out an exhaustive grid study, where three different grid levels were generated for the inner background grid and the blade grid. These have then been tried in various combinations to identify the trade-off in terms of accuracy and efficiency. In Fig. 3, the blade grids are viewed from the side along with their corresponding background grids in top view. This shows, how the background grid spacing has been gradually decreased and the outer spacing of the blade grid as well. Looking at the results in Fig. 4, it is observed that the collective pitch control angle is underestimated with respect to the experiment, but also the lateral cyclic control angle is below the experiment. While effects cannot be fully separated, the miss of collective angle is associated with the lack of elasticity, as already observed from studies with the low fidelity methods. The cyclic angle is likely associated with the lack of the fuselage as Lim and Dimanlig (Ref. 21) pointed out. Except for the CM and MC results, the overall spread of the trim control angles is little and therefore, only little differences are observed. Looking at the BVI SPL over the descent angle, it is also noted that with the increase of grid points, the results become louder and approach the experimental values, with the FF setup overestimating the experiment. While the coarse background grid benefits more from the utilization of the medium blade grid to improve the results, the medium blade grid benefits more from the utilization of the finer background mesh. Looking at the sectional load derivative in the reference descent condition in Fig. 4c, a strong growth with increasing the overall grid density is observed, which aligns with the observation of the growing noise with grid density. JAXA then selected the MM setup, with the medium blade and background grid, as it allowed for a good trade-off in speed and efficiency.

In contrast to JAXA, DLR did not investigate the interaction of different background and blade grid resolutions, but looked at three different grid sizes: 5 million grid points, 14 million grid points and 102 million grid points. The blade grid resolution is adjusted in such a way that it matches the background grid spacing, and therefore, the coarsest setup also has the least boundary layer resolution. The corresponding grid spacings are $dx/c = 20\%$, $dx/c = 14\%$, $dx/c = 7\%$. The intermediate mesh has been created by skipping every other grid point from the finest

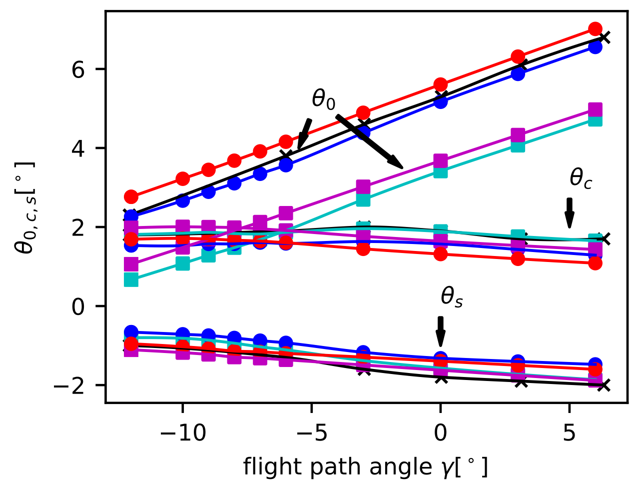

(a) Trim control angles

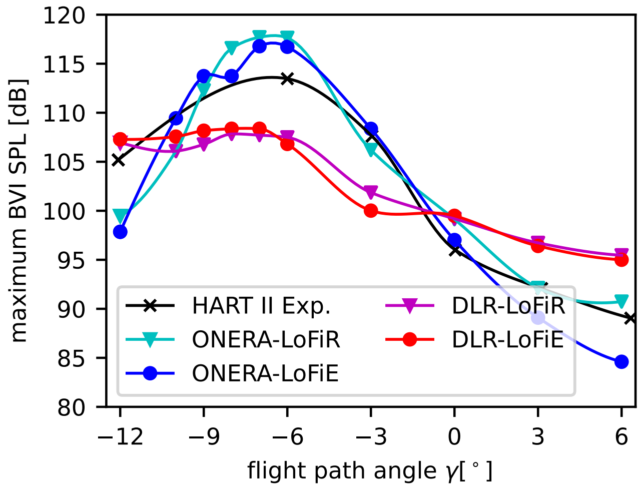

(b) Maximum blade vortex interaction sound pressure level (max. BVI SPL / only contains 6th-40th rotor harmonic)

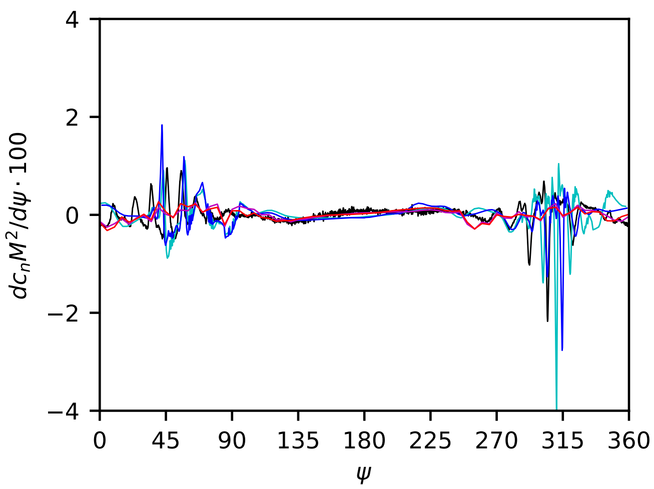

(c) Sectional normal load derivative at r/R=0.87 at $\gamma = -7.0°$

Figure 1: Baseline results by the respective partners for low fidelity methods

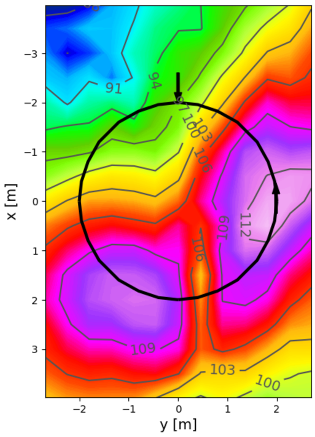

(a) Experiment

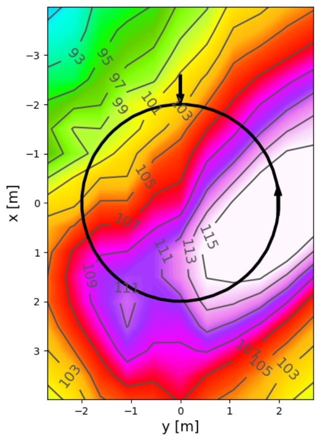

(b) ONERA LoFiR

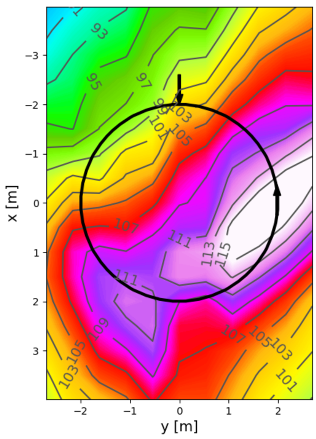

(c) ONERA LoFiE

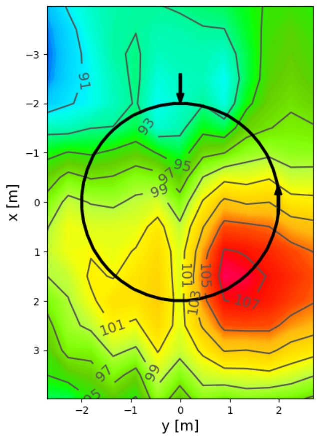

(d) DLR LoFiR

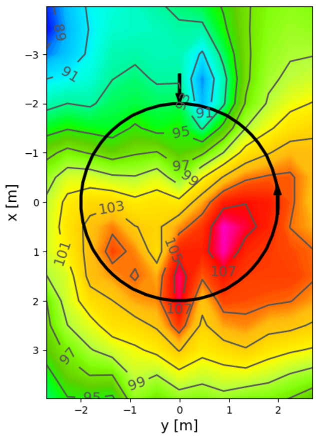

(e) DLR LoFiE

Figure 2: Baseline noise carpets by the respective partners for low fidelity methods

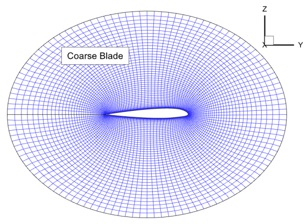

(a) Coarse blade grid from the side

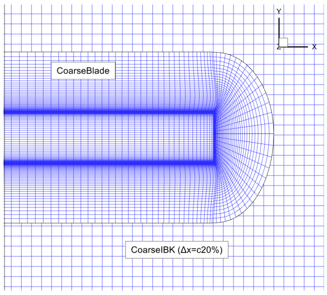

(b) Coarse blade grid in coarse background grid from top

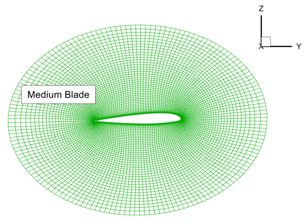

(c) Medium blade grid from the side

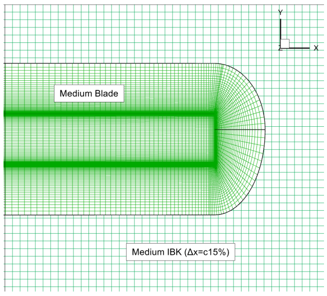

(d) Medium blade grid in medium background grid from top

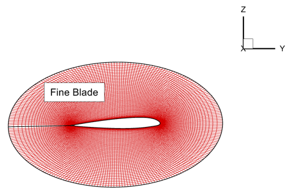

(e) Fine blade grid from the side

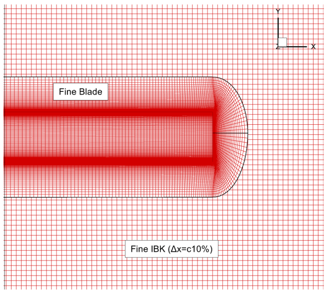

(f) Fine blade grid in fine background grid from top

Figure 3: Various grid setups generated by JAXA

mesh. The coarsest grid has been generated with different numbers, nevertheless it is built with the same process. To increase efficiency, in the background grid, partitions where no rotor wakes passed through, where coarsened once more and are connected through hanging grid nodes. Since the finest grid also has the most partitions, it reduced more grid points relatively than the other two grids. The obtained results from these three grid levels are plotted in Fig. 5. The flight control angles are not grid dependent anymore for this study, yet the aero-acoustics is still evolving. On the coarsest mesh, the peak noise is lower than the experiment, with the intermediate mesh being in almost perfect agreement and the finest mesh above the peak. In all cases, the BVI SPL is higher at the edges of the curve corresponding to a steep descent of level flight and climb. Looking at the sectional normal loads, the location of the BVI events is in good agreement with the experiment with the amplitude growing with the grid resolution. While no simulation exceeded the retreating side negative peak, on the ad-

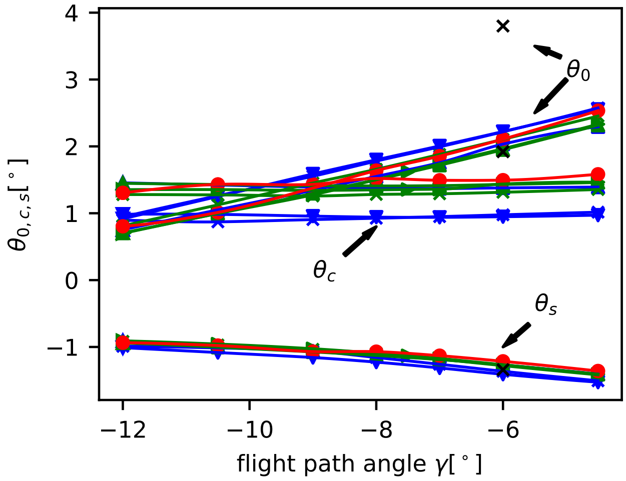

(a) Trim control angles

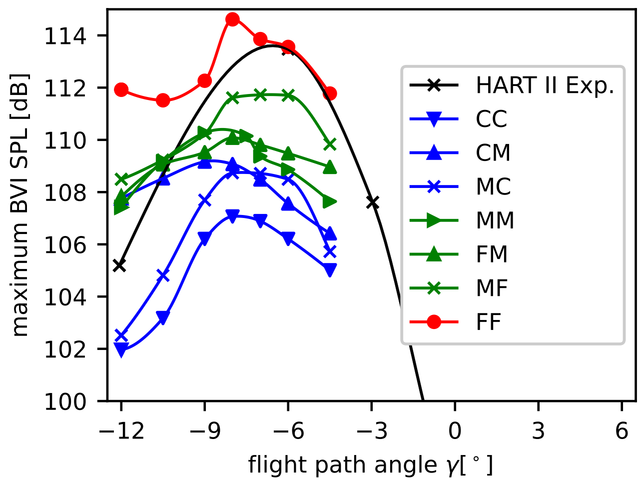

(b) Maximum blade vortex interaction sound pressure level (max. BVI SPL / only contains 6th-40th rotor harmonic)

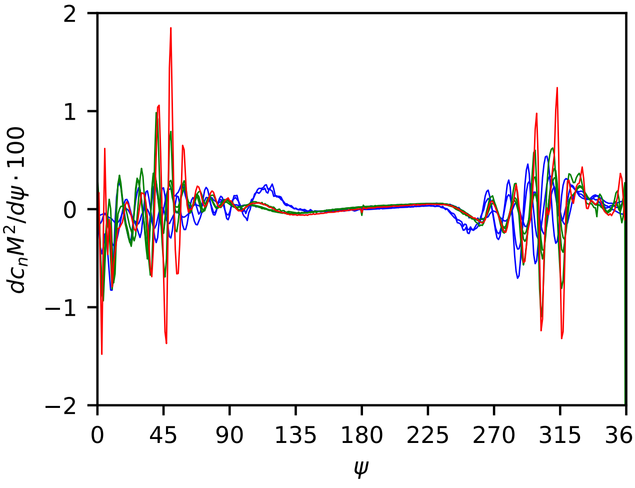

(c) normal load derivative at r/R=0.87 at $\gamma = -7.0°$

Figure 4: Baseline results from the JAXA grid study. First letter corresponds to the background grid and second latter to the blade grid. C=coarse, M=medium, F=fine, e.g. FM is the finest background grid with the medium blade grid.

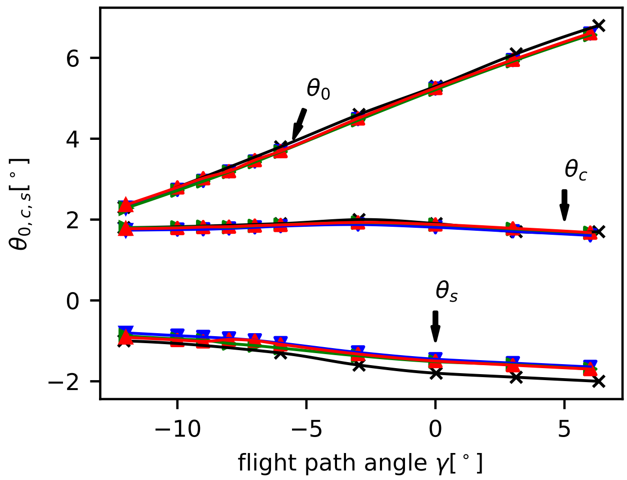

(a) Trim control angles

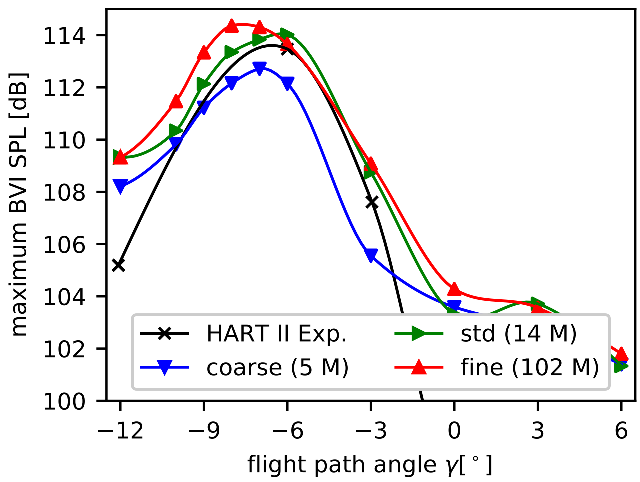

(b) Maximum blade vortex interaction sound pressure level (max. BVI SPL / only contains 6th-40th rotor harmonic)

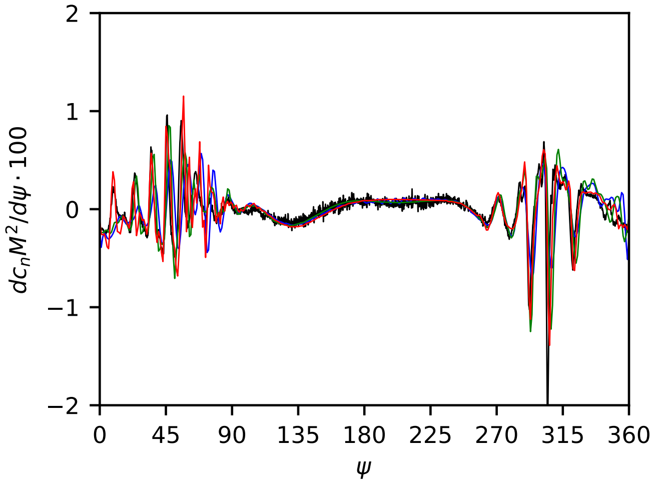

(c) Sectional normal load derivative at r/R=0.87 at $\gamma = -6.0°$

Figure 5: Baseline results from the DLR grid study

vancing side the finest grid even exceeds this peak. Due to the already good results using the intermediate mesh, the successive DLR studies in this paper have been carried out using this setup, as its computational cost is a fraction of the large mesh result. The convergence is noticeably better and the number of grid points is over a factor of eight smaller than the finest grid.

Selected Comparison

From the previous shown results, a down selection is presented and contrasted here; namely the JAXA and DLR intermediate CFD setups, the ONERA LoFiE setup, but also the ONERA CFD results previously not shown. The ONERA CFD results only consist of the data point at the reference descent angle of $\gamma = -7.0°$ for this study. The noise over descent angle and the sectional load derivative at $\gamma = -7.0°$ are given in Fig. 6. From this it is observed that there is some spread among the methods showing the challenges associated with correctly modeling descent flight. Not only need the vortices to be captured correctly from the aerodynamic solver, but also the trim control angles and elastic deformation need to match in order to obtain a good acoustic result.

Looking at the corresponding noise carpets in Fig. 7, the previous statement is further underlined. The JAXA HiFiR results capture the advancing side hot spot, but not the retreating side hot spot, which is believed to be associated with the lack of elastic modeling since the retreating side has been quieter for the rigid low fidelity methods as well. Looking at the ONERA HiFiE results, the two hot spots in the advancing and retreating sides are clearly visible. The maximum BVISPL level is underestimated, probably due to reduced grid density. Nevertheless, the directivity is satisfactory, which suggests that the locations of the interactions between the blades and the wake are correctly predicted. The ONERA results align well with the DLR results on their coarsest grid (not shown for brevity). For the DLR HiFiE results, which is the one from the standard grid, it is found that another hotspot occurs in between the existing ones. This hotspot is eminent for all three grid levels of the DLR simulation, which is also given at $\gamma = -6°$. It was already observed in Wilke (Ref. 64), yet the magnitude for this new simulation setup has increased. It is believed to be the cause of a differently resolved root vortex, as on the disc plot spurious loads are found in the aft the disc. In contrast to the previous publication, here the rotor is closed in center, but the rotor hub is neglected. Either the root vortex system deviates more from the experiment due to this, or the fuselage shields this noise in the experiment. Likely, the displacement from the fuselage pushes these vortices more into the rotor aft disc and they are not convected downward as much. While the fuselage is modeled in the aerodynamics, it has not been included in the aero-acoustic simulation.

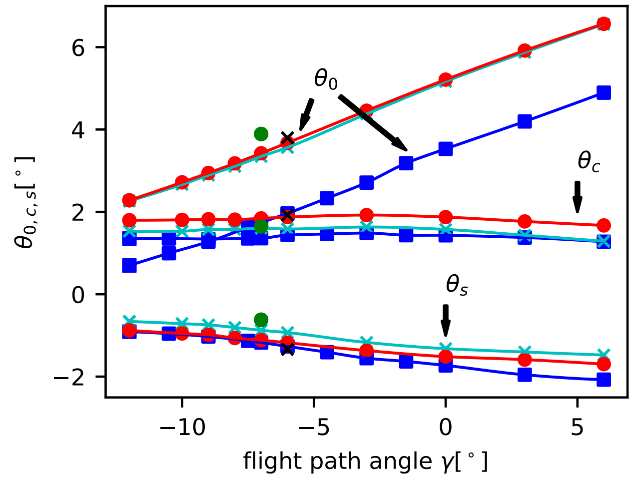

(a) Trim control angles

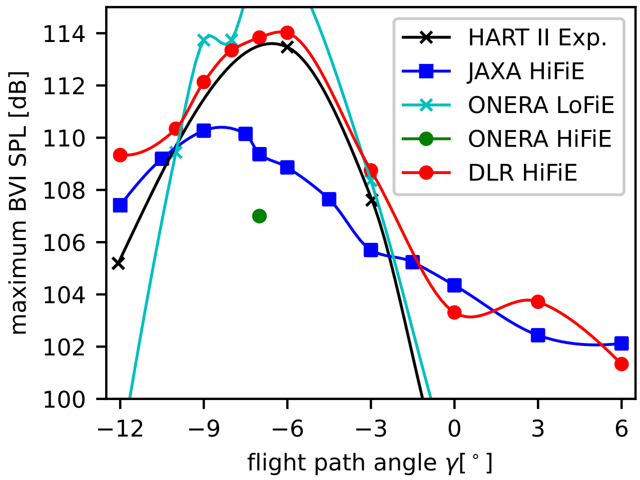

(b) Maximum blade vortex interaction sound pressure level (max. BVI SPL / only contains 6th-40th rotor harmonic)

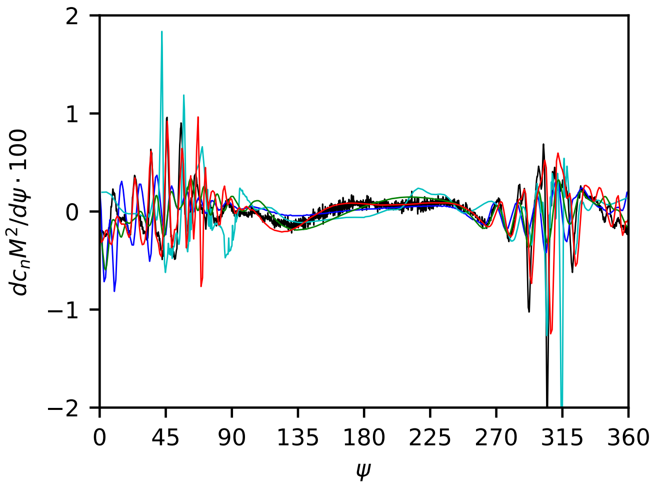

(c) Sectional normal load derivative at r/R=0.87 at $\gamma = -7.0°$

Figure 6: Baseline results for selected methods

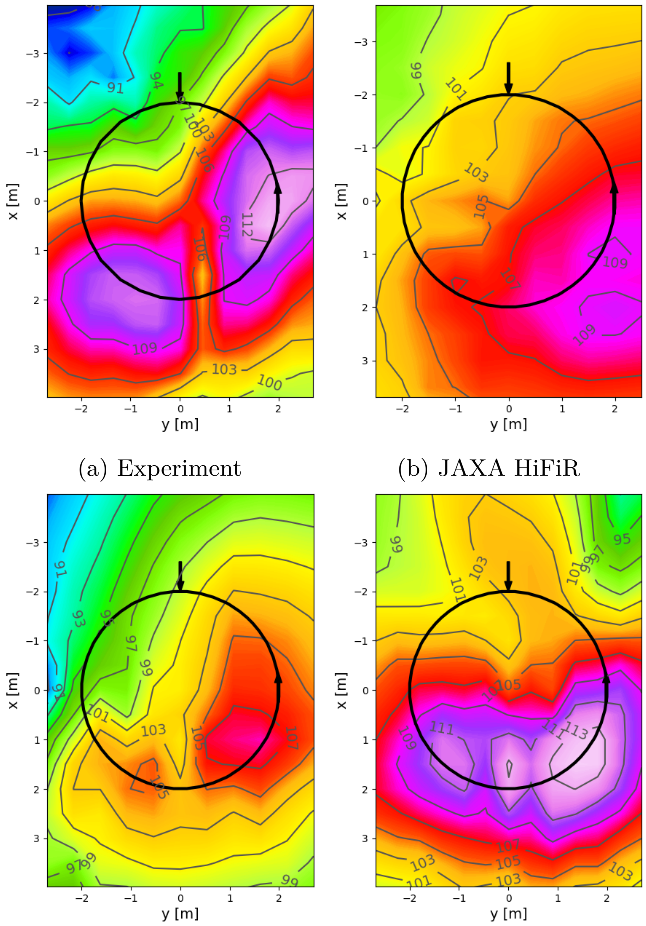

(a) Experiment

(b) JAXA HiFiR

(c) ONERA HiFiE

(d) DLR HiFiE

Figure 7: Baseline noise carpets by the respective partners for selected methods

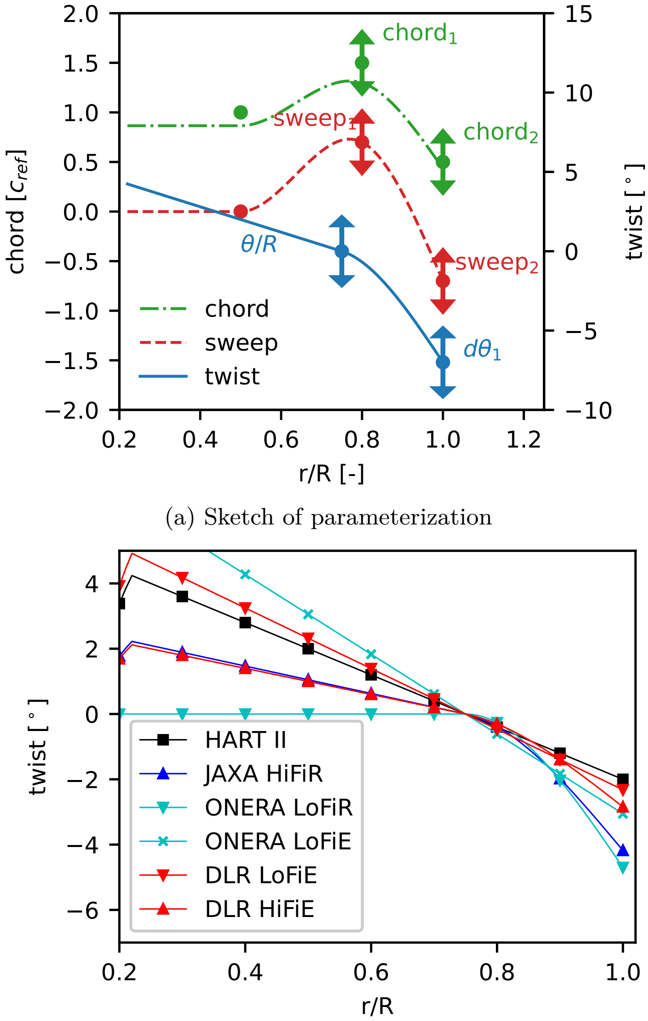

(a) Sketch of parameterization

(b) Twist distribution of optimized rotors

Figure 8: Parameterization and Twist distribution

5 Results of Blade Optimization

5.1 Optimization Problem

The overall goal is to minimize the noise heard from the rotor. The HART-II blade is a model rotor and therefore it was decided to minimize the BVI-SPL noise being associated with 6-40 rotor as this allows to transfer the results to larger rotors. Opposing this, if one would be to optimize on the A-weighted SPL noise, the results might not be transferable to full scale rotors. For simplicity, the peak-noise found on the noise carpet is to be reduced. The reference flight condition has been chosen to be $\gamma = -7°$ as it was found to be louder than $\gamma = -6°$ in the simulations. Therefore, the noise is to be minimized for this descent angle. However, during this process, DLR encountered issues, where the peak was then shifted to other angles, but remained at a similarly large values. Therefore, DLR adopted a strategy of minimizing the peak-noise for $\gamma = [-9; -6; -3]°$ degrees and use the average as the goal function for the optimizer.

The levers for reducing noise have been a total of six design variables comprising chord, sweep and twist, sketched in Fig. 8a. This parameterization is similar to the one used in the previous multi-objective optimization by the JAXA-ONERA-DLR cooperation (Ref. 3) with mainly the extension of the sweep parameter. The curves of chord, sweep and twist are all based on cubic splines. Chord and sweep both have a fixed control point at $r/R = 0.5$ where also a slope of zero is imposed. Then, at $r/R = 0.8$, a first control point is given, which the optimizer could control, followed by a last control point at the tip. The chord length has then been rescaled to match the thrust weighted solidity of the HART II rotor again. The twist parameterization consists of altering the linear twist gradient Θ/R, but has an added twist offset $\Delta\Theta_1$, which is introduced through a cubic spline at $r/R = 0.75$, where again a zero slope and value for the offset have been imposed.

The limits the optimizers were allowed to use are listed in Table 4.

Table 4: Design variables of the optimization. Chord and sweep are expressed in reference chord lengths $c_{ref} = 0.121m$.

parameter	lower bound	upper bound	baseline
$chord_1$	1.0	1.5	1.0
$chord_2$	0.5	1.0	1.0
$sweep_1$	-0.5	0.0	0.0
$sweep_2$	0.0	1.0	0.0
Θ/R	$-15.0°/R$	$0.0°/R$	$-8.0°/R$
$\Delta\Theta_1$	-10.0°	0.0°	0.0°

5.2 Obtained Blade Shapes

During the cooperation, various approaches have been tried and here only a selection is shown for brevity. The twist distributions of the optimized rotors are plotted in Fig. 8b, while the planforms are plotted in Fig. 9. The general trend of a forward-backward swept blade is captured by all designs and therefore follows the ideas of the ERATO blade (Ref. 8). Opposing this, the obtained twist distribution varies greater among the partner blades. The ONERA LoFiR has the highest linear twist gradient, while the ONERA LoFiE blade has the lowest twist gradient. For the tip twist offset, the ONERA LoFiR then features the largest negative values, where the DLR HiFiE blade has the lowest value. The JAXA HiFiR and DLR HiFiE blade have almost the same linear twist.

5.3 Cross-Validation

An important observation made already from the previous studies in the JAXA-ONERA-DLR cooperation on rotor optimization is that each partner obtains the best result with his/her respective method. Therefore, a cross-validation is carried out to identify designs that may not be the respectively best, but close enough. It is believed that a robust design should be a good design with various methods and is therefore less sensitive to uncertainties of the simulation.

For brevity, only three methods are looked into, JAXA HiFiR, ONERA LoFiE, and DLR HiFiE. The lines on the plots will refer to the method used to optimize the rotor, with the figure caption carrying the name of the method the respective results have been computed with. In Fig. 10, the BVI SPL is plotted over the descent angle for the various methods. For the rigid JAXA CFD simulations, all optimized blades show a reduction of the baseline blade for the reference case of $\gamma = -7°$. Actually, the DLR HiFiE blade slightly surpassed the JAXA HiFiR blade, but then trades places for $\gamma = -6°$. The ONERA LoFiR blade reduces the peak the least and it is shifted towards lower descent angles. Moving onto the ONERA results, the elastic ONERA optimized blade performs well for the found targeted condition, yet shifts the noise peak to steeper descent angles. Conversely, the

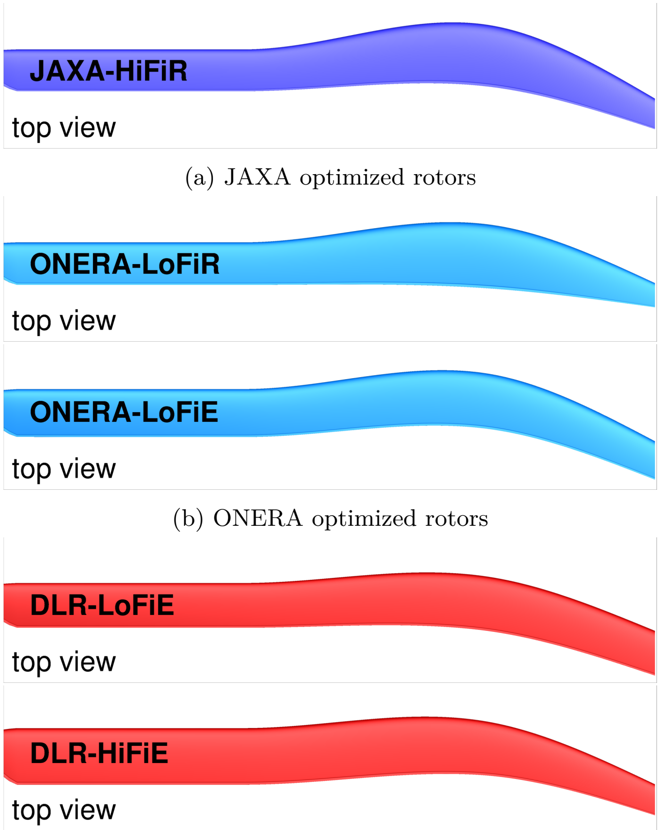

(a) JAXA optimized rotors

(b) ONERA optimized rotors

(c) DLR optimized rotors

Figure 9: Top view of optimized rotors. The blade name refers to the method they have been optimized with

JAXA and DLR blades shift their peaks to more shallow angles. Nevertheless, in all case the maximum noise is reduced over the baseline blade. For DLR, the high-fidelity optimized blade DLR HiFiE is best according to the three point averaged metric, but it shows a larger peak at $\gamma = -6..-7°$ than the ONERA LoFiE and the DLR LoFiE blades. The ONERA LoFiE blade shows a similar tendency as already observed when evaluated ONERA LoFiE method that the peak is shifted towards steeper descent angles. The DLR optimized blades show a second peak at climb angles. The JAXA blade improves noticeably for steeper descent angles, but actually becomes louder than the baseline blade for angles larger than $\gamma > -6°$, with the ONERA LoFiR showing a similar behavior.

In Fig. 11, the derivative of the normal load is shown for the r/R=0.87 cut computed with the individual methods by each partner. Among all methods, the JAXA HiFiR methods has the smallest amplitudes of the BVI. Also, the reduction of amplitudes for the optimized blades is not seen between 0..45°, but becomes better visible for 45..90° on the advancing side. On the retreating side, DLR HiFiE blade shows the largest amplitudes after the HART II blade, with the ONERA LoFiR blade showing the smallest amplitudes. For the ONERA LoFiE method, it is observed that the JAXA HiFiR blade and ONERA

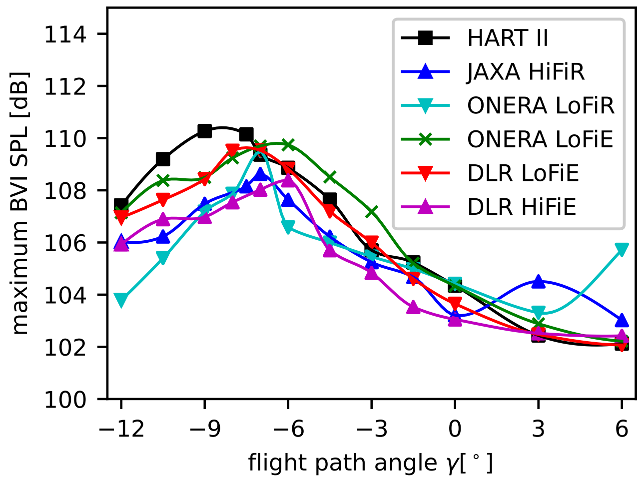

(a) Computed with JAXA HiFiR

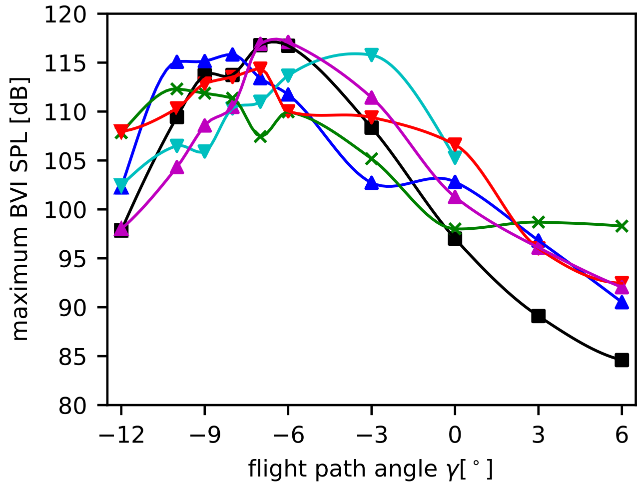

(b) Computed with ONERA LoFiE

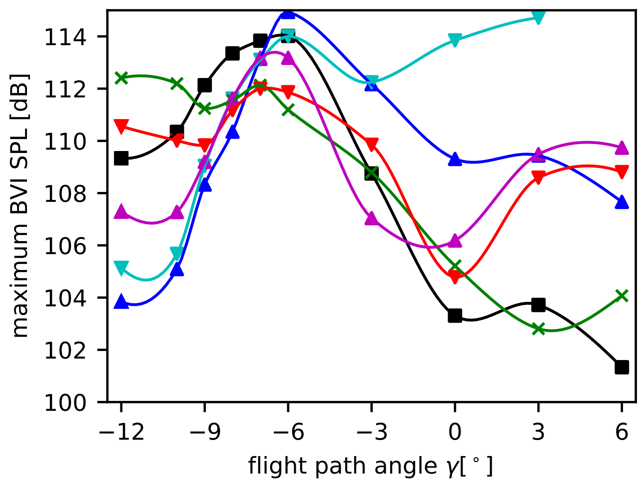

(c) Computed with DLR HiFiE

Figure 10: Descent angle sweep of optimized rotors

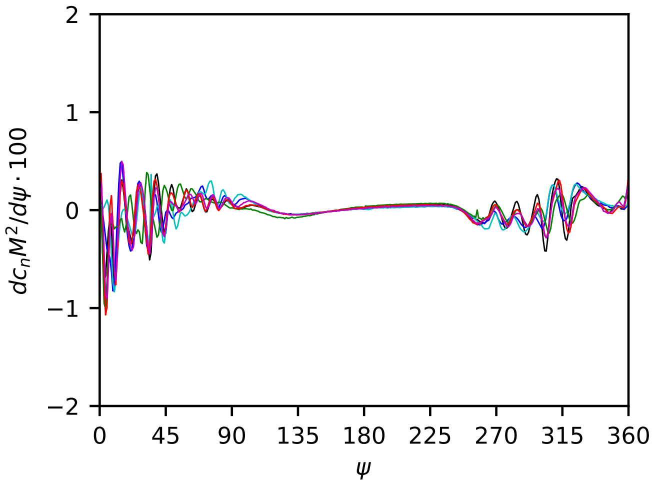

(a) Computed with JAXA HiFiR

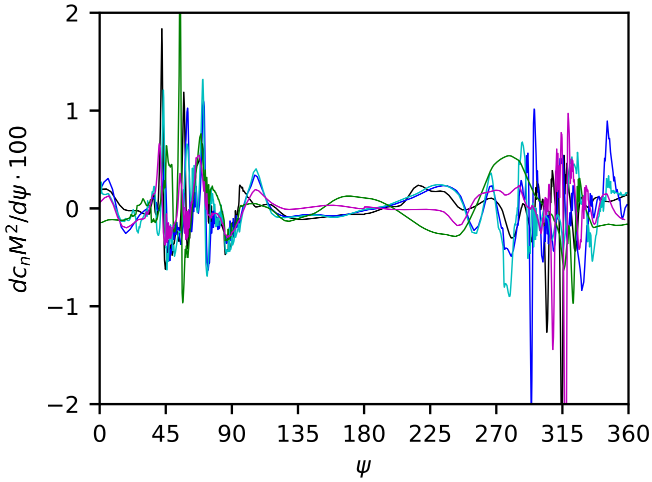

(b) Computed with ONERA LoFiE

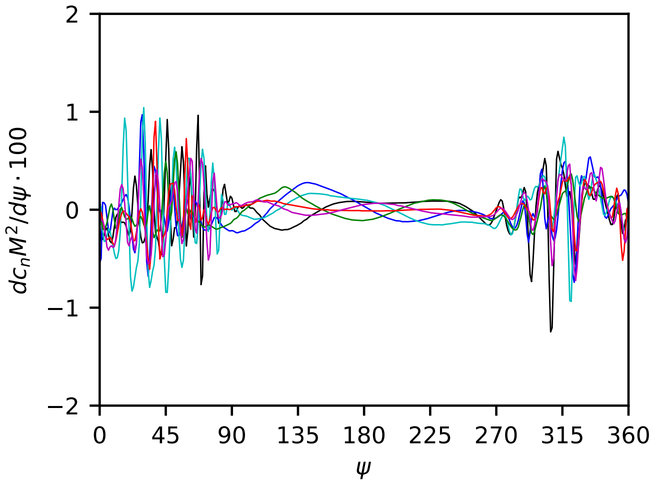

(c) Computed with DLR HiFiE

Figure 11: Sectional normal load derivative at r/R=0.87 at $\gamma = -7.0°$

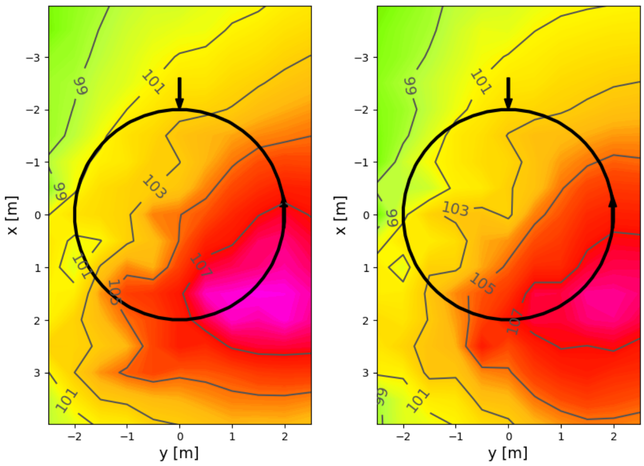

(a) JAXA HiFiR blade (b) DLR HiFiE blade

Figure 12: Noise carpet of respective blades computed with JAXA HiFiR at $\gamma = -7.0°$

LoFiE blade perform well, whereas the DLR HiFiE blade shows a strong peak on the retreating side being even larger than the HART II peak. However, since the advancing side is mildly quieter the peak noise on the carpet just arrives close the HART II blade, but for this blade, the retreating side hot spot is louder. Moving onto the results for the DLR HiFiE method, the reduction of the peaks is not as strong for the optimized blades, but still visible. The JAXA HiFiR blade exhibits similarly strong peaks as the HART II blades matching the found observation from the descent angle sweep. The ONERA LoFiR blade, the advancing side shows peaks in the magnitude of the HART II blade, but on the retreating side, a similar magnitude is observed. The DLR LoFiE and ONERA LoFiE blades have reduced peaks in contrast and are on a similar level in this flight condition. The DLR HiFiE has mildly reduced peaks over the DLR LoFiE and ONERA LoFiE blades, but only mildly, which correlates with the findings on the angle sweep.

The noise carpets of the JAXA HiFiR and DLR HiFiE blade are plotted in Fig. 12 and Fig. 13 when computed with the JAXA HiFiR method and the DLR HiFiE method respectively to further understand why the JAXA blade has relatively high levels of noise when computed with DLR HiFiE, but not when computed with JAXA HiFiR. The JAXA HiFiR retrieves very similar noise carpets with a reduction of the 107 dB area for the DLR HiFiE blade over the JAXA HiFiR blade. For DLR HiFiE, it is observed that this blade has a strong advancing side hot spot, with an inexistent retreating side hot spot, but also a new noise location in front of the rotor. It is found to grow stronger for level flight, and is becoming noticeably stronger for the ONERA LoFiR blade. The reason for this could be traced back to too strong torsional elastic deformation due to an excitation of the 1^{st} torsion mode of these blades.

Thus, the tip torsion deformation is exemplary plotted in Fig. 14 for $\gamma = 3°$, where the ONERA LoFiR blade exceeds the noise of the HART II blade, but also the JAXA and DLR blades become louder again. While the JAXA HiFiR exhibits the largest overall deformation, its peak-to-peak value $\Delta\theta_{el} = 8.6°$ is reduced over the ONERA LoFiR blade $\Delta\theta_{el} = 9.5°$. This means that it features a high static torsion offset that does not cause noise by itself and only changes directivity. The ONERA LoFiR blade shows a stronger peak-to-peak variation, which then shows a strong impact on the noise carpet similar to the JAXA HiFiR blade in descent flight, yet corresponding to the front peak found for the JAXA blade. Without doing a true re-design of the blade interior, the elastic properties obtained from the simplified Stanger scaling approach used by DLR for the DLR HiFiE blade are projected onto the JAXA HiFiE and ONERA LoFiR blades as it showed the lowest torsion peak-to-peak value of $\Delta\theta_0 = 4.6°$ after the HART II blade ($\Delta\theta_0 = 1.6°$). This is simply due to the fact that the DLR HiFiE design has the largest inboard chord length and therefore obtains the highest torsional rigidity. These blade structural properties shift the 1^{st} torsion eigenmode frequency to 3.27 $\omega_{mode}/\Omega_{rotor}$ for the JAXA HiFiR blade and to 2.88 $\omega_{mode}/\Omega_{rotor}$ for the ONEA LoFiR blade to 4.45 $\omega_{mode}/\Omega_{rotor}$ for the DLR HiFiE blade at nominal RPM when computed with the HOST model. For reference, the HART II blade has the 1^{st} torsion eigenmode frequency at 4.05 $\omega_{mode}/\Omega_{rotor}$ in the HOST computation, whereas the non-rotating experimental value is at 3.5 $\omega_{mode}/\Omega_{rotor}$. While also close to the $4n/rev$ for HOST, it seems that the HART II blade is not as much excited due to being a rectangular blade without sweep.

This means the effect of elasticity is non-negligible for the aero-acoustic blade design. While one could reinforce the inner sections of the JAXA HiFiR and ONERA LoFiR blades, they feature the slimmest inner sections due to the thrust weighted solidity scaling. Therefore, it is more complicated to achieve high torsional rigidity

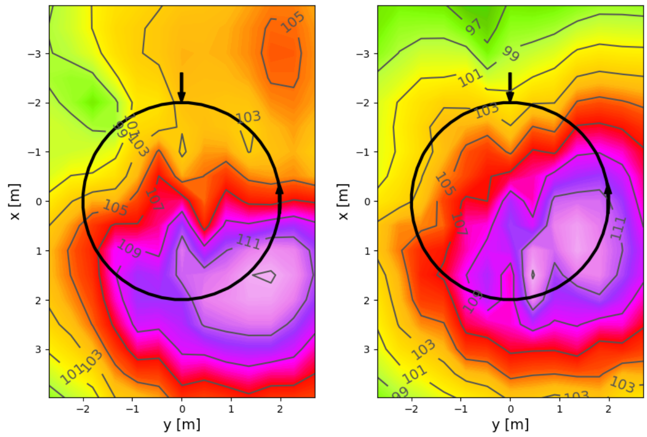

(a) JAXA HiFiR blade (b) DLR HiFiE blade

Figure 13: Noise carpet of respective blades computed with DLR HiFiE at $\gamma = -7.0°$

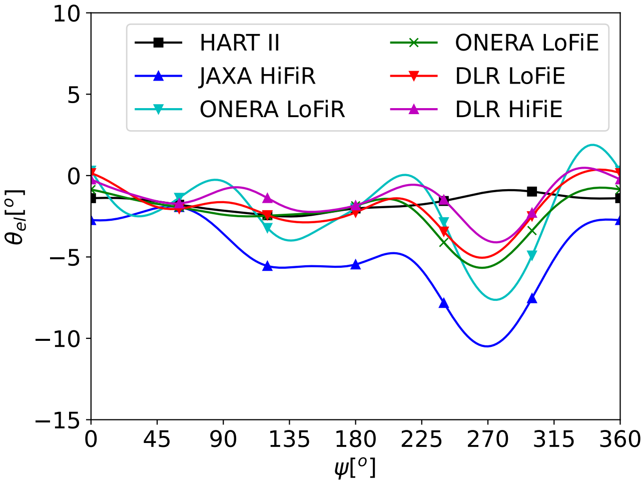

Figure 14: Tip torsion deformation of optimized blades for $\gamma = 3.0^\circ$ when computed with DLR HiFiE

than in contrast to the DLR HiFiE blade, which features the thickest inboard section of all optimized blades and therefore shows the smallest peak-to-peak deformation after the HART II blade and followed by the ONERA LoFiE blade.

6 Conclusions & Recommendations

In the fourth work package of the JAXA-ONERA-DLR rotor optimization cooperation, the noise of a rotor blade in descent flight is to be minimized exclusively. Therefore, the methods available to the partners have first been verified against the renowned HART II rotor. The outcome of these studies it that even with low-fidelity methods, trends can already be captured well, but even well adapted coarse CFD grids may already capture the trends, yet at a too quiet level. The best results were obtained by using a well resolved CFD simulation and including the elastic deformation, but also the fuselage.

Moving forward and optimizing the noise of the HART II rotor, good agreement on the planform could be found with the various methods, but large differences on the twist angles are obtained. Cross-validating the individual blades with the respectively other blades revealed mixed results. While the rigid CFD method could show that all optimized blades were actually reducing the noise, the elastic low fidelity and elastic CFD methods showed that rigidly optimized blades become louder. The issue could be pinpointed to too strong torsion deformations, which would become even louder than the plain BVI noise. As for the elastically optimized rotors, these designs could reduce the peak noise, but the peak position also often shifted to either steeper descent angles or climb flight. Using a three-point approach to minimize the noise throughout various descent angles allowed to robustly reduce the noise, but did not necessarily lead to the overall best design as not all descent angles were included. Contrasting this with the ERATO blade (Ref. 8), the behavior of a shifted peak has already been observed there, where the peak noise was shifted towards level flight in comparison with the 7AD blade. While the double-swept blade changes the reception of the tip vortex on the blade as well as the miss-distance, it does not allow to do so for all angles as the BVI then occurs at other angles.

As a recommendation, all methods have shown their merits, but a careful cross-check with a well resolved CFD method including elasticity is advised before progressing further with the design. Preferably, a structural layout matching the outer mold line of the rotor is already considered, as elasticity has an impact on the rotor acoustics.

Future research in the JAXA-ONERA-DLR cooperation plans to cross-over the power reduction in hover and forward flight with this acoustic condition to arrive at a good all-around blade design.

7 Aknowledgements

The DLR authors gratefully acknowledge the scientific support and HPC resources provided by the German Aerospace Center (DLR). The HPC system CARA is partially funded by "Saxon State Ministry for Economic Affairs, Labour and Transport" and "Federal Ministry for Economic Affairs and Climate Action". The HPC system CARO is partially funded by "Ministry of Science and Culture of Lower Saxony" and "Federal Ministry for Economic Affairs and Climate Action".

8 Copyright Statement

9 References

1. G. Wilke, J. Bailly, K. Kimura, and Y. Tanabe, "JAXA-ONERA-DLR Cooperation: Results from Rotor Optimization in Hover," CEAS Aeronautical Journal, Vol. 13, 2022, pp. 313–333. DOI: 10.1007/s13272-022-00580-8.

2. K. Kimura, G. Wilke, J. Bailly, Joëlle, and Y. Tanabe, "JAXA-ONERA-DLR Cooperation: Results from Rotor Optimization in Forward Flight," 48th European Rotorcraft Forum, September 2022.

3. J. Bailly, G. Wilke, K. Kimura, and Y. Tanabe, "JAXA-ONERA-DLR Cooperation: Results from Multi-Point Aerodynamic Optimization of a Rotor in Hover and Forward Flight," 49th European Rotorcraft Forum, September 2023.

4. W. R. Splettstößer, G. Niesl, F. Cenedese, F. Nitti, D. G. Papanikas, "Experimental Results of the European HELINOISE Aeroacoustic Rotor Test," 19th European Rotorcraft Forum, 1993.

5. J. Prieur, and W. R. Splettstößer, "ERATO- an ONERA-DLR Cooperative Programme on Aeroacoustic Rotor Optimisation," 25th European Rotorcraft Forum, 1999.

6. Y. Delrieux, J. Prieur, M. Costes, P. Gardarein, P. Beaumier, H. des Rochettes, P. Leconte, W. R. Splettstößer, B. van der Wall, B. Junker, K.-J. Schultz, E. Mercker, and K. Pengel, "The ONERA-DLR Aeroacoustic Rotor Optimisation Programme ERATO: Methodology and achievements," AHS Aerodynamics, Acoustics, and Test and Evaluation Technical Specialists Meeting, 2002.

7. M. Allongue and J.P. Drevet, "New rotor test rig in the large Modane wind tunnel," 15th European Rotorcraft Forum, 1989.

8. B.G. van der Wall, C. Kessler, Y. Delrieux, P. Beaumier, M. Gervais, J-F Hirsch, K. Pengel, and P. Crozier, "From ERATO Basic Research to the Blue Edge Rotor Blade," AHS International 72nd Annual Forum & Technology Display, May 2016.

9. D. Alfano, P. Cranga, V. Gareton, F. Guntzer, and J-F Hirsch, "The Blue Edge™Blade Continuation," Proceedings of the 75th Annual Forum, May 2019.

10. A. Brocklehurst, and G. N. Barakos, "A review of helicopter rotor blade tip shapes," Progress in Aerospace Sciences, Vol. 56, (0), 2013, pp. 35–74. DOI: 10.1016/j.paerosci.2012.06.003.

11. B. G. van der Wall, "A Comprehensive Rotary-Wing Data Base for Code Validation: The HART II International Workshop," The Aeronautical Journal, Vol. 115, (1164), 2011, pp. 91–102.

12. N. Kobiki, Y. Tanabe, T. Aoyama, D. H. Kim, H. J. Kang, Y. W. Seung, and H.Kim, "Design, Analysis and Prototyping of Active Tab Rotor," 41st European Rotorcraft Forum, 2015.

13. B. G. van der Wall, J. W. Lim, J. Riemenschneider, S. Kalow, G. Wilke, and D. D. Boyd, Jr., J. Bailly, Y. Delrieux, I. Cafarelli, Y. Tanabe, H. Sugawara, S. N. Jung, S. H. Hong, D.-H. Kim, H. J. Kang, G. Barakos, and R. Steininger, "Smart Twisting Active Rotor (STAR) - Pre-Test Predictions," 48th European Rotorcraft Forum, September 2022.

14. P. Küfmann, R. Bartels, B. G. van der Wall, O. Schneider, H. Holthusen, J. Gomes, and J. Postma, "The First Wind Tunnel Test of the DLR's Multiple Swashplate System: Test Procedure and Preliminary Results," AHS 72nd Annual Forum, 2016.

15. K. S. Brentner, and F. Farassat, "Modeling Aerodynamically Generated Sound of Helicopter Rotors," Progress in Aerospace Sciences, Vol. 39-2, 2003, pp. 83–120.

16. H. E. Jones, and C. L. Burley, "A Study of the Effects of Blade Shape on Rotor Noise," AHS Technical Specialists' Meeting for Rotorcraft Acoustics and Aerodynamics, 1997.

17. T. Brooks, C. Burley, D. Boyd, Jr. and J. Jolly, Jr., Aeroacoustic codes for rotor harmonic and BVI noise - CAMRAD.Mod1/HIRES, 1996. DOI: 10.2514/6.1996-1735.

18. G. Rahier, and Y. Delrieux, "Blade-Vortex Interaction Noise Prediction Using a Rotor Wake Roll-Up Model," Journal of Aircraft, Vol. 34, (4), July 1997, pp. 522–530. DOI: 10.2514/2.2204.

19. P. Beaumier, and Y. Delrieux, "Description and Validation of the ONERA Computational Method for the Prediction of Blade-Vortex Interaction Noise," Aerospace Science and Technology, Vol. 9, (1), 2005, pp. 31–43. DOI: http://dx.doi.org/10.1016/j.ast.2004.07.008.

20. E.P.N. Duque, L.N. Sankar, S. Menon, O. Bauchau, S. Ruffin, M. Smith, K. Ahuja, K.S. Brentner, L.N. Long, P.J. Morris, and F. Gandhi, "Revolutionary Physics-Based Design Tools for Quiet Helicopters," 44th AIAA Aerospace Sciences Meeting and Exhibit, 2006.

21. J. W. Lim, and A. C. B. Dimanlig, "The Effect of Fuselage and Rotor Hub on Blade-Vortex Interaction Airloads and Rotor Wakes," 36th European Rotorcraft Forum, 2010.

22. B. G. van der Wall, J. W. Lim, M. J. Smith, S. N. Jung, J. Bailly, J. D. Baeder, and D. D. Boyd, Jr., "The HART II International Workshop: An Assessment of the State-of-the-Art in Comprehensive Code Prediction," CEAS Aeronautical Journal, Vol. 4, (3), 2013, pp. 223–252. DOI: 10.1007/s13272-013-0077-9.

23. M. J. Smith, J. W. Lim, B. G. van der Wall, J. D. Baeder, R. T. Biedron, D. D. Boyd Jr, B. Jayaraman, S. N. Jung and B-Y Min, "An assessment of CFD/CSD prediction state-of-the-art using the HART II international workshop data," 68th Annual Forum of the American Helicopter Society, 2012.

24. M. Sugiura, Y. Tanabe, S. Saito, H. Sugawara, K. Ohshio, and M. Kanazaki, "Hybrid Method of CFD and Prescribed Wake Model for Rotorcraft Aeroacoustics and Aerodynamics Prediction," 38th European Rotorcraft Forum, 2012.

25. R. K. Jain, J. W. Lim, and B. Jayaraman, "Modular Multisolver Approach for Efficient High-Fidelity Simulation of the HART II Rotor," Journal of American Helicopter Society, 2015.

26. U. Kowarsch, C. Öhrle, M. Keßler, and E. Krämer, "Aeroacoustic Simulation of a Complete H145 Helicopter in Descent Flight," Journal of the American Helicopter Society, Vol. 61, (4), 2016, pp. 042001–1 – 042001–13.

27. G. Wilke, "Efficient Aero-Acoustic Simulation of the HART II Rotor with the Compact Pade Scheme," 42nd European Rotorcraft Forum, 2016.

28. G. Wilke, "Progress in Aero-Acoustic Optimization Techniques in DLR's VicToria Project," ONERA-DLR Aerospace Symposium 2019, January 2019.

29. G. Wilke, Aerodynamic Optimization of Helicopter Rotorblades using Variable Fidelity Methods, Ph.D. thesis, Technische Universität Braunschweig, 2017.

30. Y. Hong, S. H. Park, and K. Yee, "Comparative Assessment of Local Accuracy of High-Order Spatial Schemes for Rotorcraft Aeroacoustics," AIAA Journal, Vol. 61, (1), 2023, pp. 355–377. DOI: 10.2514/1.J062008.

31. J. D. Baeder, "Passive Design for Reduction of High-Speed Impulsive Rotor Noise," 52nd Annual Forum of the American Helicopters Society, 1996.

32. A. Visingardi, L. Federico, and M. Barbarino, "Blade Planform Optimization for a Dual Speed Rotor Concept," 38th European Rotorcraft Forum, 2012.

33. D. Rabe, Parameter studies for the aeroacoustic design of helicopter rotors based on different methods, Master's thesis, TU Braunschweig, 2017.

34. D. Rabe and G. Wilke, "Parametric Design Studies of the Helicopter Rotor Noise using Variable-Fidelity Methods," AHS International 74th Annual Forum & Technology Display, May 2018.

35. E. Fabiano, and D. Mavriplis, "Adjoint-Based Aeroacoustic Design-Optimization of Flexible Rotors in Forward Flight," Journal of Americal Helicopter Society, Vol. 62-4, (042005), 2017, pp. 1–17. DOI: 10.4050/jahs.62.042005.

36. L. Wang, B. Diskin, L. V. Lopes, E. J. Nielsen, E. Lee-Rausch, and R. T. Biedron, "High-Fidelity AeroAcoustic Optimization Tool for Flexible Rotors," Journal of the American Helicopter Society, Vol. 66, (022004), 2020, pp. 1–116.

37. T. A. Fitzgibbon, Advanced Rotor Blade Design based on High-Fidelity Computational Fluid Dynamics, Ph.D. thesis, College of Science and Engineering, University of Glasgow, 2021. DOI: 10.5525/gla.thesis.81932.

38. T. A. Fitzgibbon, M. A. Woodgate, G. N. Barakos, and R. H. Markiewicz, "Rotor-Blade Planform Design Based on an Overset Harmonic-Balance-Adjoint Optimization Framework," AIAA Journal, Vol. 59, (9), 2021, pp. 3431–3447. DOI: 10.2514/1.J060175.

39. M. H. Chia, K. Duraisamy, A. K. Padthe, and P. P. Friedmann, "Active and Passive Helicopter Noise Reduction Using the AVINOR/HELINOIR Code Suite," Journal of Aircraft, Vol. 55, (2), March 2018, pp. 727–740. DOI: 10.2514/1.c034519.

40. G. Reboul, J. Bailly, L. Rottmann, P. Bekemeyer, G. Einarsson, and F. Guntzer, "Prediction of RACER's Lateral Rotor Noise Using the CONCERTO Chain," Proceedings of the 77th Annual Forum, May 2021.

41. F. Guntzer, J. Caillet, C. Cariou, J.-P. Pinacho, P. Dieumegard, and E. Roca León, "A Comprehensive Helicopter Acoustic Modeling Tool based on Simulation and Experiment," 49th European Rotorcraft Forum, 2023.

42. J.P. Yin, and S. R. Ahmed, "Helicopter Main-Rotor/Tail-Rotor Interaction," Journal of the American Helicopter Society, Vol. 45, (4), 2000, pp. 293–302.

43. P. Spiegel, G. Rahier, and B. Michea, "Blade-vortex interaction noise - Prediction and comparison with flight and wind tunnel tests," 18th European Rotorcraft Forum, September 1992.

44. B. Benoit, A.-M. Dequin, K. Kampa, W. von Grünhagen, P.-M. Basset, and B. Gimonet, "HOST, a General Helicopter Simulation Tool for Germany and France," 56th Annual Forum of the American Helicopters Society, May 2000.

45. J. Yin, and J. Delfs, "Improvement of DLR Rotor Aeroacoustic Code (APSIM) and its Validation

with Analytic Solution," 29th European Rotorcraft Forum, 2003.

46. P. Spiegel, and G. Rahier, "Theoretical study and prediction of BVI noise including close interactions," AHS Technical Specialists Meeting onRotorcraft Acoustics and Fluids Mechanics, Vol. -1, 04 1991.

47. J. Raddatz, and J. K. Fassbender, "Block Structured Navier-Stokes Solver FLOWer," MEGAFLOW - Numerical Flow Simulation for Aircraft Design, edited by N. Kroll and J. K. Fassbender, 2005.

48. Y. Tanabe, S. Saito, and H. Sugawara, "Validation of High Resolution CFD Analysis For Flowfield Around a Rotor," The 40th Japan Society for Aeronautical and Space Sciences Annual Meeting, 2009.

49. L. Cambier, S. Heib, and S. Plot, "The Onera elsA CFD Software: Input from Research and Feedback from Industry," Mechanics & Industry, Vol. 14, (3), 2013, pp. 159–174. DOI: 10.1051/meca/2013056.

50. S. Yamamoto, S. Kano, and H. Daiguji, "An Efficient CFD Approach for Simulating Unsteady Hypersonic Shock-Shock Interference Flows," Computers & Fluids, Vol. 27, (5), 1998, pp. 571–580. DOI: 10.1016/S0045-7930(97)00061-3.

51. G. Wilke, "Comparisons of Different Spatial Schemes and Limiters for Helicopter Flows," New Results in Numerical and Experimental Fluid Mechanics XIII, edited by A. Dillmann, G. Heller, E. Krämer, and C. Wagner, 2021. DOI: 10.1007/978-3-030-79561-0.

52. K. Kitamura, and E. Shima, "Towards shock-stable and accurate hypersonic heating computations: A new pressure flux for AUSM-family schemes," Journal of Computational Physics, Vol. 245, 2013, pp. 62–83. DOI: 10.1016/j.jcp.2013.02.046.

53. A. Jameson, W. Schmidt, and E. Turkel, "Numerical Solution of the Euler Equations by Finite Volume Methods Using Runge-Kutta Time-Stepping Schemes," 14th AIAA Fluid and Plasma Dynamics Conference, 1981. DOI: 10.2514/6.1981-1259.

54. I. Petropoulos, M. Costes, and P. Cinnella, "Development and analysis of high-order vorticity confinement schemes," Computers & Fluids, Vol. 156, Ninth International Conference on Computational Fluid Dynamics (ICCFD9), 2017, pp. 602–620. DOI: 10.1016/j.compfluid.2017.04.011.

55. S. Allmaras, F. T. Johnson, and P. Spalart, "Modifications and clarifications for the implementation of the Spalart-Allmaras turbulence model," Seventh International Conference on Computational Fluid Dynamics (ICCFD7), January 2012.

56. J. Dacles-Mariani, D. Kwak, and G. Zilliac, "On numerical errors and turbulence modeling in tip vortex flow prediction," International Journal for Numerical Methods in Fluids, Vol. 30, (1), 1999, pp. 65–82. DOI: 10.1002/(SICI)1097-0363(19990515)30:1<65::AID-FLD839>3.0.CO;2-Y.

57. P. R. Spalart, S. Deck, M. Shur, K. D. Squires, M. Kh. Strelets, and A. Travin, "A New Version of Detached-eddy Simulation, Resistant to Ambiguous Grid Densities," Theoretical and Computational Fluid Dynamics, Vol. 20, (3), May 2006, pp. 181. DOI: 10.1007/s00162-006-0015-0.

58. F. R. Menter, M. Kuntz, and R. Langtry , "Ten years of industrial experience with the SST turbulence model," Heat and Mass Transfer, Vol. 4, (1), 2003, pp. 625–633. DOI: 10.1.1.460.2814.

59. J. C. Kok, "Resolving the Dependence on Freestream Values for the k- Turbulence Model," AIAA Journal, Vol. 38, (7), 2000, pp. 1292–1295. DOI: 10.2514/2.1101.

60. C. C. Heister, "A Method for Approximate Prediction of Laminar-Turbulent Transition on Helicopter Rotors," Journal of the American Helicopter Society, Vol. 63, (3), July 2018, pp. 1–14.

61. D. Krige, "A Statistical Approach to some Mine Valuation and allied Problems on the Witwatersrand", Ph.D. thesis, University of the Witwatersrand, 1951.

62. D. R. Jones, M. Schonlau, and W. J. Welch, "Efficient Global Optimization of Expensive Black-Box Functions," Journal of Global Optimization, Vol. 13, 1998, pp. 455–492.

63. Y. Tanabe, and S. Saito, "Significance of All-Speed Scheme in Application to Rotorcraft CFD Simulations," The 3rd International Basic Research Conference on Rotorcraft Technology, 2009.

64. G. Wilke, "Findings in Aero-Acoustic Simulations for Optimizations," AHS International 76th Annual Forum, October 2020.

65. M. Costes, "Development of a 3rd-order Vorticity Confinement Scheme for Rotor Wake Simulations," 38th European Rotorcraft Forum, 2012.

66. C. B. Allen, "CHIMERA volume grid generation within the EROS code," Proceedings of the Institution of Mechanical Engineers, Part G: Journal of Aerospace Engineering, Vol. 214, 2000, pp. 125–140. DOI: 10.1243/0954410001531962.

67. B. G. van der Wall, S. N. Jung, J. W. Lim, M. J. Smith, J. Bailly, J. D. Baeder, and D. D. Boyd, Jr., "An Assessment of Comprehensive Code Prediction State-of-the-Art Using the HART II International Workshop Data," Annual Forum 68 of the American Helicopter Society, 2012.